AOfPR

Asian and Oceanic Forum for Paediatric Radiology

Vol. 8
July 2024

AOSPR Annual Scientific Meeting 2023 was held successfully in the Hong Kong Academy of Medicine on 2-3 September 2023. Despite being challenged by the untimely typhoon on the first day, the quick-witted Organising Committee seamlessly transformed the event to a hybrid virtual and physical meeting. The Meeting brought together more than 300 healthcare professionals from over twenty countries, international and local specialists in paediatric radiology gathered and shared knowledge. Networking was forged, nurturing passion in the field and building foundations for future collaborations.

The 2-day scientific programme embraced diverse topics ranging from neuroimaging to musculoskeletal radiology, from interventional radiology to quality and safety. There were four multi-disciplinary sessions on oncological imaging, imaging in renal disease, neuro radiology and state-of-the art imaging. Apart from the invited lectures delivered by the outstanding speakers from around the world, the proffered papers sessions, hands-on workshops and film quiz were equally popular.

In this issue, we include four excellent presentations that were awarded in AOSPR 2023. We express our gratitude to the authors for their outstanding contributions and generous acceptance of our invitation for publication in this issue of AOfPR.

Enjoy the forum!

Professor Winnie Chu
Congress Co-Chairperson
Organising Committee AOSPR 2023

Dr. Elaine Kan
Congress Co-Chairperson
Organising Committee AOSPR 2023

Paper no: 20

Predicting response to initial chemotherapy in pediatric lymphoma using a semi quantitative CECT-based abdomino-thoracic score:

a pilot prospective observational study.

Ishan Kumar, MBBS, MD, DNB
Department of Radiodiagnosis and Imaging,
Institute of Medical Sciences, Banaras Hindu University, Varanasi, India

Co-authors: Shashank Sonkar, Priyanka Aggarwal, Vineeta Gupta, Ram Chandra Shukla, Ashish Verma

Background

Pediatric Lymphoma: third most common malignancy of childhood

Imaging modalities: US, Contrast Enhanced CT, FDG-PET, PET-CT, Whole body MRI

CT scan has become the standard of care in pre-treatment staging

Do not emphasize the estimation of lymph nodal disease burden based on the anatomical extent of the nodal involvement

Purpose

To validate a **semiquantitative lymph nodal scoring system** based on the anatomical pattern of involvement to

- Systematically estimate the ***burden*** of thoraco-abdominal lymph nodal disease in childhood lymphoma
- to ***predict response*** to the primary therapy
- to distinguish ***HL and NHL***

Methods

prospective observational study

Children (<18 years of age) with a histopathological diagnosis of lymphoma

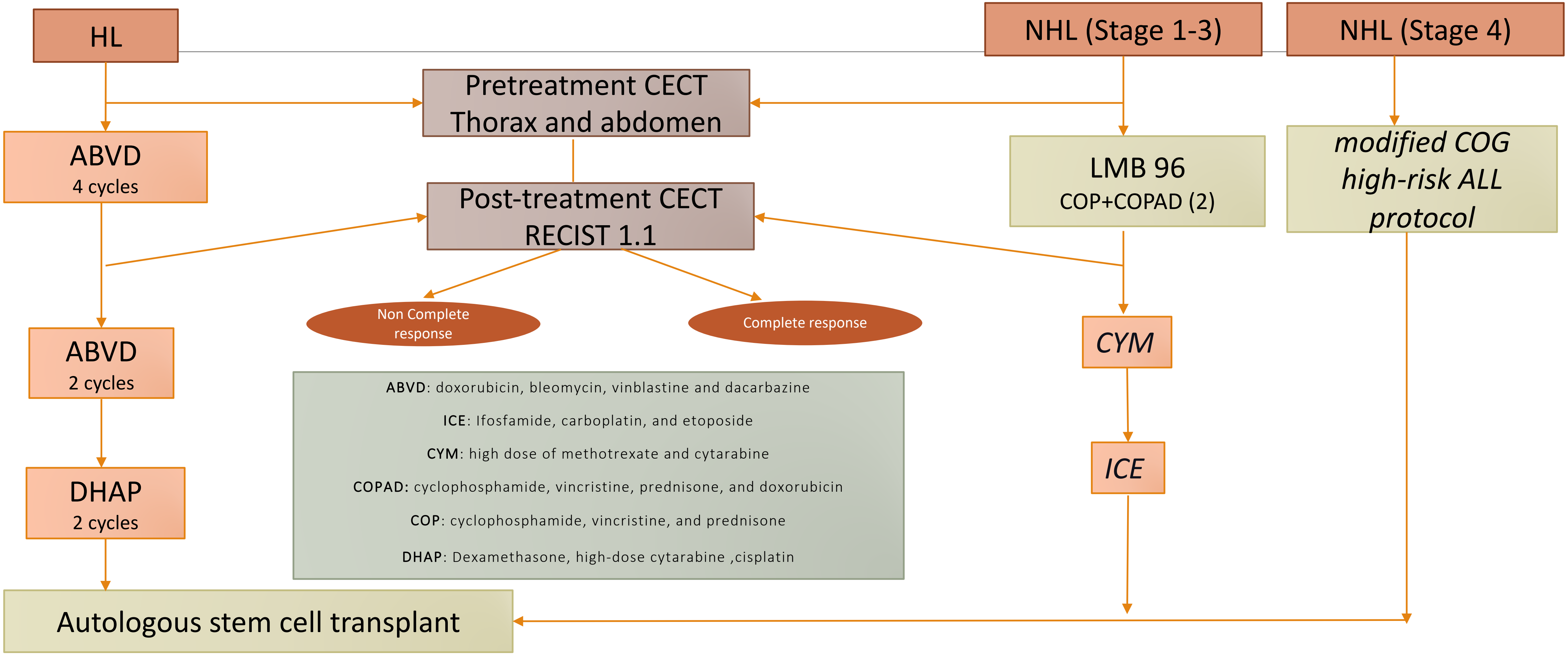

ABVD: doxorubicin, bleomycin, vinblastine and dacarbazine

ICE: Ifosfamide, carboplatin, and etoposide

CYM: high dose of methotrexate and cytarabine

COPAD: cyclophosphamide, vincristine, prednisone, and doxorubicin

COP: cyclophosphamide, vincristine, and prednisone

DHAP: Dexamethasone, high-dose cytarabine ,cisplatin

Combined score (total score 20): Thoracic score + Abdominal score

THORACIC SCORE (SCORE 10)

- Superior mediastinal
- Paratracheal
- Subaortic
- Paraaortic
- Subcarinal
- Para esophageal
- Pulmonary ligament
- Hilar
- Interlobar
- Chest wall & axillary LN

ABDOMINAL SCORE (SCORE 10)

- Abdominal wall LN
- Diaphragmatic LN
- Liver
- Stomach
- Pancreatic LN
- Mesenteric LN
- Colon LN
- Suprarenal retroperitoneal LN
- Infrarenal retroperitoneal LN
- Pelvic LN

Region	LN stations
Abdominal wall LN	*Anterior* Superficial: supraumbilical LN/infraumbilical LN Deep: superior epigastric pathway/inferior epigastric pathway/intercostal pathway *Posterior* Superficial: LN along superficial circumflex vessels Deep: LN along lumbar arteries/LN along deep circumflex iliac artery
Diaphragmatic LN	Anterior diaphragmatic LN/middle diaphragmatic LN/retrocrural LN/inferior diaphragmatic LN
Liver	Cystic duct LN/gastrohepatic/hepaticoduodenal LN/falciform ligament LN/falciform ligament/deep superior epigastric LN (subxiphoid)
Stomach	At lesser curvature: right paracardial LN/lesser curvature LN/suprapyloric nodes At greater curvature: left paracardial/proximal left greater curvature LN/distal left greater curvature LN/right greater curvature LN/infrapyloric LN Near lesser curvature: left gastric artery LN/common hepatic artery LN/celiac trunk LN/left hepatoduodenal ligament LN/posterior hepatoduodenal ligament LN/foramen of Winslow LN
Pancreas	Pancreaticoduodenal LN: anterior/posterior/inferior Dorsal pathway posterior to pancreatic head: superior/ inferior Body/tail: along proximal splenic artery/along distal splenic artery/splenic hilar LN
Mesenteric LN (small bowel)	Juxtaintestinal LN/intermediate mesenteric nodes/central mesenteric LN
Colon	Cecum: periappendiceal/ anterior cecal/ posterior cecal Colon: epicolic LN/ paracolic LN/intermediate mesocolic/terminal colic LN • Intermediate mesocolic LN: ileocolic LN/right colic LN/middle colic LN/left ascending and descending colic LN/ left colic LN/LN along sigmoidal artery • Terminal colic LN: SMA/IMA/middle colic Perirectal LN: sigmoid mesocolon LN/mesorectal LN Perianal LN: above pectinate line/below pectinate line
Retroperitoneal	Retrocaval LN/ precaval LN/laterocaval LN/aortocaval LN/preaortic LN/retroaortic LN/lateral aortic LN • Level: aortic hiatus LN/ middle paraaortic/ caudal paraaortic Perirenal: renal hilar/suprahilar/posterosuperior perirenal LN/posteroinferior perirenal LN
Pelvic	Common iliac LN: lateral/medial/middle External iliac LN: lateral/middle/obturator Internal iliac LN: Junctional/ anterior/iliac circumflex/lateral circumflex Perivisceral: • perivesical: prevesical/postvesical/lateral vesical • periuterine/parametrial/pericervical LN • periprostatic/ periseminal vesicle LN Others: posterior iliac crest LN/ gonadal vessels LN Inguinal LN: superficial/ deep inguinal LN

Regional abdominal pattern scores

Gastric nodal score : total score 9

Celiac axis -peripancreatic : total score 13

Mesentrico-colic score: total score 14

Retroperitoneal score : Total score 17

Kumar et al.
Indian J Radiol Imaging. 2022;32(1):62-70.

Results

Fifty patients : Mean age of 7.56 ± 3.01 years (M: F= 39:11).

- Hodgkin lymphoma (HL) : 35
- Non Hodgkin lymphoma (NHL) : 15

Comparison between HL and NHL

Lymph nodes/ nodal score	HL	NHL	p-value
Abdominal score	3.5±2.3	4.8±2.1	0.035
Thoracic score	3.3±1.75	5.2±2.8	0.026
Combined score	6.89±3.54	10.0±3.96	0.01

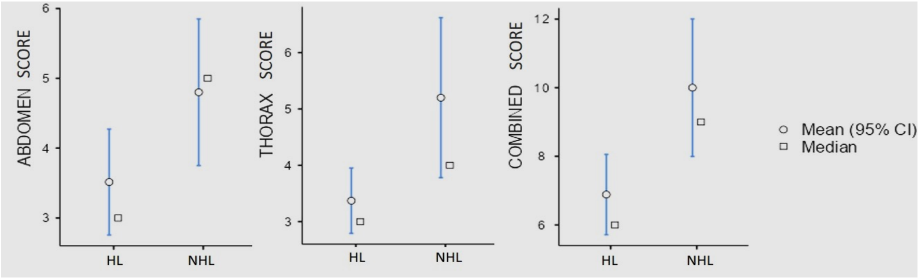

Thorax			
Upper paratracheal	5 (14%)	6 (40%)	0.44
Lower paratracheal	7 (20%)	8 (53%)	0.018
Pulmonary ligament	4 (11.4%)	7 (47%)	0.006

Lymph nodes/ nodal score	HL	NHL	p-value
Mesenteric			
Juxta-intestinal	18 (51%)	13 (87%)	0.019
Intermediate	18 (51%)	13 (87%)	0.019
Central	17(51.4%)	12 (80%)	0.039
Retroperitoneal			
Latrocaval	18 (51%)	13 (87%)	0.019
Aortocaval	19 (54%)	14 (93%)	0.008
Preaortic	19 (54%)	14 (93%)	0.008
Retroaortic	20 (57%)	14 (93%)	0.012
Lateral aortic	21 (60%)	14 (93%)	0.018
Aortic hiatus	21 (60%)	14 (93%)	0.018
Middle paraaortic	20 (57%)	14 (93%)	0.012
Caudal paraaortic	19 (54%)	14 (93%)	0.008
Renal hilar	20 (57%)	13 (87%)	0.043
Suprahilar	17(51.4%)	13 (87%)	0.012
Posterosuperior perirenal	16 (46%)	13 (87%)	0.007
Posteroinferior perirenal	16 (46%)	12 (80%)	0.025
Retroperitoneal score (total 17)	7.51±5.92	12.4±3.89	0.005

Response assessment in HL and NHL

Lymph nodes/score	Complete response	Non complete response	P value
	Hodgkin Lymphoma		
HL (n=35)	23(65.7%)	12 (34.3%)	
Mean abdominal score	2.48±1.56	5.50±2.20	**<0.001**
Mean thorax score	2.78 ± 1.31	4.50 ± 1.98	**0.016**
Combined score	5.26 ±2.09	10.00± 3.72	**<0.001**
Regional abdominal scores			
Celiac axis-pancreatic	0.95 ±1.6	4.92± 4.29	**<0.001**
Retroperitoneal score	6.27± 6.017	9.25 ± 5.38	0.163
Mesentrico-colic score	4.50 ± 5.6	11.42 ± 4.87	**0.001**
Gastric score	0.046 ± 0.21	1.58 ± 3.03	**0.022**
	Non-Hodgkin Lymphoma		
NHL (n=15)	6 (40%)	9 (60%)	
Mean abdominal score	3.67 ± 0.52	5.56± 2.40	**0.012**
Mean thorax score	2.67 ±0.82	6.89 ± 2.32	**<0.001**
Combined score	6.33 ± 0.82	12.44 ±3.21	**<0.001**

Children with complete response in both HL and NHL group showed a lower thoracic, abdominal, and combined scores than those who did not show complete response to primary treatment.

Discussion

This study is the first one to elaborate on the differences in the nodal pattern of involvement between HL and NHL

Points favoring NHL

- **Higher nodal burden** : higher thoracic, abdominal and combined scores
- Higher involvement of **retroperitoneal and mesenteric** lymph nodes
    - Increased incidence of IVC compression
- Higher incidence of enlarged **upper and lower paratracheal**, and pulmonary ligament LN
    - Increased Airway compression

Study	Modality	Lymph nodal staging system	Reference
Cotswolds modifications of the Ann Arbor staging (Hodgkin lymphoma)	CT	4 stages: • single LN, • $\geq$ 2 LN ipsilateral to diaphragm, • LN on both sides of the diaphragm a • diffuse disease with 1 extralymphatic organ bulky disease: > 10 cm or $\geq$1/3rd of transverse thoracic diameter on Chest X ray -PA view.	J Clin Oncol. 1989;7: 1630-1636.
International Pediatric Non-Hodgkin Lymphoma Staging System (IPNHLSS)	CT	4 stages • Single LN (exclusion of abdomen/chest) • $\geq$ 2 LN ipsilateral to diaphragm • $\geq$ 2 LN both sides of diaphragm/ chest involvement • CNS/ bone marrow involvement	J Clin Oncol. 2015;33(18):2112-2118.
La Fougere et al, 2006	PET-CT	7 regions: cervical, thoracic, abdominal , pelvic, bone marrow, extra-nodular and spleen.	Eur J Nucl Med Mol Imaging. 2006;33:1417-1425
Freudenberg et al, 2004	PET-CT	11 regions: cervical, supraclavicular, paratracheal, mediastinal, hilar, axillary, coeliac, para-aortic, mesenteric, iliac and inguinal Four anatomical groups: (1) head and neck, (2) chest, (3) abdomen and (4) pelvis.	Eur J Nucl Med Mol Imaging. 2004;31:325-329
EuroNet-PHL	CT or MRI	Bulky disease: Volume measurements of the contiguous mediastinal Adenopathy >200 mL • software-based volumetry • multiplanar volume reconstruction : (AxBxC)÷2	Pediatr Radiol. 2019;49(11):1545-1564
Brennan et al	CT WB-MRI	Thorax (8 regions): anterior mediastinum, right paratracheal, right tracheobronchial, left paratracheal, left tracheobronchial, aortopulmonary window, subcarinal, and epicardial regions Abdomen (5 regions) : Paraaortic, mesenteric, iliac and pelvic sidewall, inguinal, visceral	Am J Roentgenol. 2005;185(3):711-716.
Sabri et al	MRI	Thorax (10 regions): Paratracheal, Prevascular, Paraaortic, Subaortic, Hilar, Sub carinal, Para esophageal, Cardiophrenic, Internal mammary, Supra clavicular	Egypt J Radiol Nucl Med 2021; 52: 215
Present study	CT	Thorax (10 regions) Abdomen (10 regions)	

Conclusions

Semiquantitative scoring of lymph nodal distribution

- *A better estimate of extent of disease*
  - *offers both diagnostic and prognostic value*

Limitations

- *low number of included patients*
- *CT instead of PET-CT*
- *the non-inclusion of cervical lymph nodes*
- *Did not assess interobserver agreement*

AOSPR 2023
21st Annual Scientific Meeting of Asian and Oceanic Society for Paediatric Radiology
2nd-3rd SEPTEMBER
HONG KONG
Hong Kong Academy of Medicine Jockey Club Building
Organised by

Abstract No.: 129

Title: Milder Motor Impairment is Associated with Less Extensive Thalamic Damage in Full-term Children with PVL

Author(s): Jieqiong Lin, Hongwu Zeng

Affiliation(s): Shenzhen Children's Hospital

Background

- Periventricular leukomalacia (PVL) is a common neuroimaging feature in individuals with spastic cerebral palsy. Difference in microscopic alterations in grey matter (GM) between premature and full-term children with PVL is still unclear.
- To investigate the impact of ischemic and hypoxic events on microstructure through analyzing GM changes in cerebral palsy patients with PVL, including premature PVL(pPVL) and full-term PVL (fPVL).

Purpose and Methods

pPVL (n=27) fPVL (n=15) HC (n=38)

*Gross Motor Function Measure (GMFM)

*Fine Motor Function Measure (FMFM)

Voxel-Based Morphometry and Structural Covariance Network Analysis

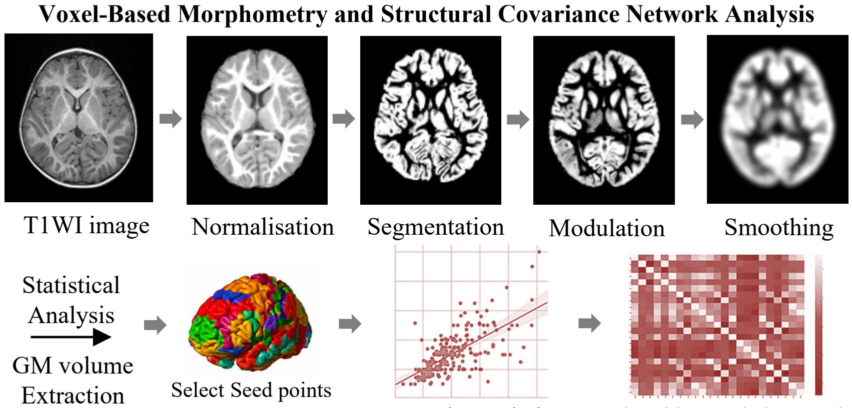

Results & Conclusion(s)

- Compared to the HC, there were reductions of total intracranial volume, GM, and white matter (WM) volume in the pPVL group, also reduced volume in bilateral thalamic; only reduced volume in the left thalamic volume within the fPVL group (p<0.001).
- Correlation analysis showed a stronger association of thalamic volume changes with gross motor function scores in pPVL groups.

Table 1 Regions of significant volume differences between PVL and Healthy controls (HC > PVL)

Anatomical Region	MNI coordinates X	Y	Z	voxel	p-value FWE corrected
PVL versus HC					
Left thalamus	-29	-21	29	2460	<.0001
Right thalamus	27	-33	30	2298	<.0001
pPVL versus HC					
Left thalamus	-14	-21	9	2446	<.0001
Right thalamus	17	-23	15	2342	<.0001
fPVL versus HC					
Left thalamus	-9	-21	11	2044	<.0001
Left Lentiform Nucleus	-20	-4	7	172	<.0001

Cluster threshold set at 100 voxels using p<.0001;Brain regions are based on AAL atlas. FWE, family wise error; MNI, Montreal Neurological Institute

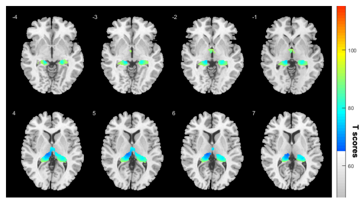

Fig 1. Comparison of GM volumes between the whole PVL group and HC group at a threshold of P<0.0001 (FWE corrected).

Fig 2. Bilateral thalamus, precentral gyrus, postcentral gyrus, SMA, Superior parietal lobule, paracentral lobule, caudate, putamen, pallidum, and cerebellum were selected as seed points in structural covariance network analysis.

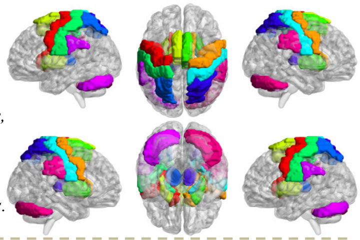

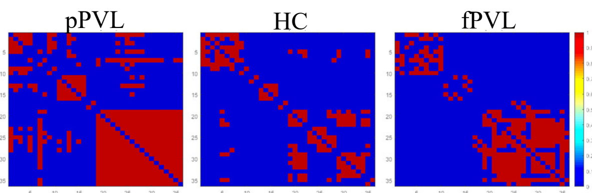

Fig 3. Structural correlation matrix of pPVL, HC and fPVL group according to the selected seed points in brain regions.

- Compared with the HC group, the structural association of gray matter volume between right thalamus and right posterior central gyrus increased in pPVL group, and the structural association between thalamus and cerebellar hemisphere increased in fPVL group.
- Compared with the fPVL group, the structural association between right thalamus-cerebellar hemisphere in pPVL group tends to decrease.

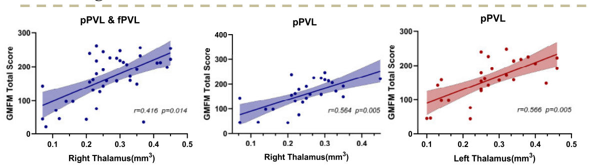

Fig 4. Correlation between GM volume and motor scores in PVL and PVL subtypes

Conclusions: Preterm and full-term PVL children have different thalamic volume changes, as well as abnormalities in the structural covariance network associated with the thalamus.

AOSPR 2023
21st Annual Scientific Meeting of Asian and Oceanic Society for Paediatric Radiology
2nd-3rd SEPTEMBER
HONG KONG
@ Hong Kong Academy of Medicine Jockey Club Building
Organised by AOSPR

Abstract No. : 24

Abstract Title: A Pictorial Review of Cardiac MRI Features in Post COVID-19 Vaccine Acute Myocarditis

Authors: Dr. CT Wang, Dr. HL Tsui, Dr. PY Chu, Dr. YH Hui, Dr. YW Hon
Affiliation: Department of Radiology & Organ Imaging, United Christian Hospital

醫院管理局 HOSPITAL AUTHORITY
基督教聯合醫院 UNITED CHRISTIAN HOSPITAL

Background

- Post COVID-19 vaccine acute myocarditis was reported since commencement of vaccination program in Hong Kong. Cardiac MRI (CMR) played a key role in diagnosis.

Purpose and Method

- To review myocardial injury pattern after COVID-19 vaccine on CMR.
- Patients under 18 years old with clinically suspected post COVID-19 vaccine acute myocarditis were included between 1/1/2021 and 28/2/2023. CMR images were reviewed with reference to Lake Louise Criteria 2009.

Lake Louise Criteria 2009

Main criteria	1. Edema ➔ Regional or global **signal intensity (SI) increase** in **T2**-weighted images. 2. Hyperaemia/ Capillary Leak ➔ Regional or global **early Gadolinium enhancement** in **T1**-weighted images. 3. Necrosis/ Fibrosis ➔ At least one focal lesion with **non-ischaemic regional distribution** on **late Gadolinium enhancement**.
Supportive criteria	1. Left ventricular dysfunction 2. Pericardial involvement

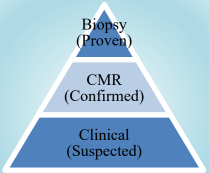

Level of evidence in diagnosing myocarditis

- ❖ If **at least 2 out of 3** main criteria present → **consistent with acute myocarditis**
- ❖ If **only 1 out of 3** main criteria present → still suggestive of acute myocarditis in **appropriate clinical scenario** and **supportive criteria**

Results & Conclusion

Gender	12 male, 3 female
Age (Mean)	12-17 years old (14.7 years old)
Time interval from vaccination to presentation (Mean)	0-13 days (2.9 days)
No. of patients with elevated cardiac enzymes	Troponin T: 7/15 (46.7%) Creatinine Kinase: 3/15 (20%)
Type of vaccine	BioNTech : 15/15 (100%)

Table 1. Characteristics of the 15 patients with clinically suspected post COVID-19 vaccination myocarditis

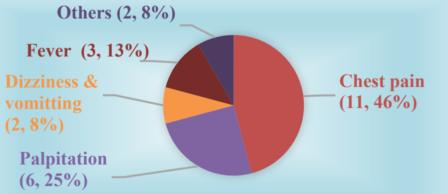

Fig 1. Symptoms of the 15 patients after BioNTech vaccine.

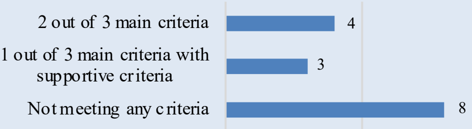

Fig 2. 7 out of 15 patients showed CMR features of acute myocarditis.

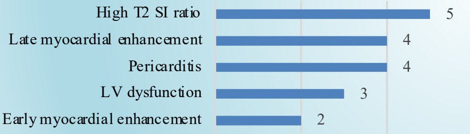

Fig 3. CMR features of the 7 patients with acute myocarditis.

Conclusion

Recognising **Cardiac MRI** features of **post COVID-19 vaccine myocardial injury pattern** with **clinical** and **biochemical** evidence of acute myocarditis will facilitate prompt treatment in our paediatric patients.

2 out of 3 main criteria

Fig 4. 16/F with palpitation.
A-B. T2-weighted dark blood short axis view
Transmural global T2 hyperintensity seen within myocardium.
C-D. T1-weighted short axis view with Gadolinium enhancement
Patchy early Gadolinium enhancement at basal anterior, basal anteroseptal, basal inferior and apical septal segments (arrows).

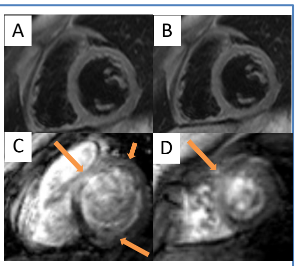

Fig 5. 13/M with chest pain and fever.
A. T2-weighted dark blood short axis view.
Transmural T2 hyperintensity seen within myocardium at basal inferior segments (arrowheads).
B-D. T1-weighted short axis view with Gadolinium enhancement
Regional late Gadolinium enhancement at basal inferior and basal infero-lateral segments (arrows) with subepicardial or midwall involvement.

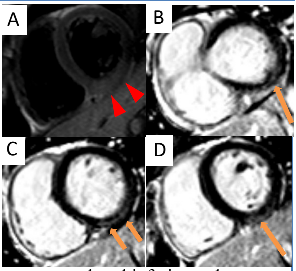

1 out of 3 main criteria with supportive criteria

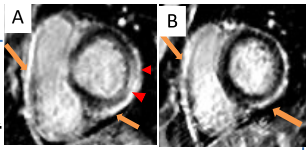

Fig 6. 17/M with chest pain and fever.
A-B. T1-weighted short axis view with Gadolinium enhancement
Regional late Gadolinium enhancement at basal infero-lateral segment with subepicardial and midwall involvement (arrowheads).
Abnormal pericardial thickening with late Gadolinium enhancement indicates pericarditis (arrows).

Fig 7. 17/M with chest pain and palpitation.
A. T2-weighted dark blood short axis view
Transmural global T2 hyperintensity seen within myocardium.

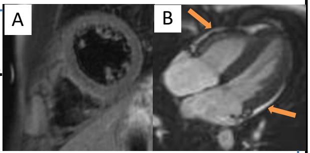

B. T2-weighted 4 chamber view
Mild pericardial effusion (arrows).

The authors have no conflict of interest to disclose with respect to this presentation.

Reference:
1 Fronza, M., Thavendiranathan, P., Chan, V., Karur, G. R., Udell, J. A., Wald, R. M., Hong, R., & Hanneman, K. (2022, September). Myocardial Injury Pattern at MRI in COVID-19 Vaccine–Associated Myocarditis. *Radiology*, *304*(3), 553–562. https://doi.org/10.1148/radiol.212559
2. Law, Y. M., Lal, A. K., Chen, S., Čiháková, D., Cooper, L. T., Deshpande, S., Godown, J., Grosse-Wortmann, L., Robinson, J. D., & Towbin, J. A. (2021, August 10). Diagnosis and Management of Myocarditis in Children. *Circulation*, *144*(6). https://doi.org/10.1161/cir.0000000000001001

AOSPR 2023 21st Annual Scientific Meeting of Asian and Oceanic Society for Paediatric Radiology
2nd-3rd SEPTEMBER
HONG KONG 香港 @ Hong Kong Academy of Medicine Jockey Club Building
Organised by AOSPR

Abstract No. 8

Milky CSF? A Rare Case of Catheter-related Extensive IVC Thrombosis in a Neonate

Dr Leanne HQ Chin[1], Dr Derek LH Chan[1], Dr Christy YK Mak[2], Dr Christopher CH Tong[2], Dr Khair Jalal[2], Dr Alan KS Chiang[2]
[1]Department of Radiology, Queen Mary Hospital, Hong Kong SAR
[2]Department of Paediatrics & Adolescent Medicine, Queen Mary Hospital, Hong Kong SAR

Background:
Neonatal inferior vena cava (IVC) thrombosis can result from extrinsic compression from oncologic pathology, iatrogenic thrombus or in-utero thrombosis. Due to broad and non-specific clinical presentation, epidemiology remains indeterminate, which may mean a significant portion are underrecognized but has significant implications on short- and long-term morbidity and mortality.

Objectives & Methods: *Case report*
In this exhibit, we report an unusual presentation of IVC thrombosis secondary to **repeated** central venous catheter (CVC) insertion (Fig 1) in a preterm neonate, presenting with sepsis, generalized oedema, abdominal distension and dilated superficial abdominal veins. Septic workup including lumbar puncture yielded abnormal milky content (Fig 2), suspicious for total parenteral nutrition (TPN) extravasation.

Initial imaging including ultrasound (US) and magnetic resonance imaging (MRI) of lumbosacral (L-S) spine was unrevealing except for relatively prominent epidural venous plexus. However, further scrutiny of the retroperitoneal area in the included field of view (FOV) of MRI revealed absence of IVC flow void with irregular contour and T2 heterogeneity (Fig 3).

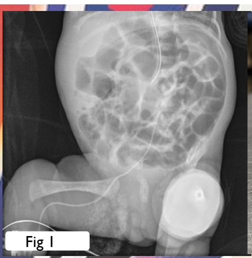
Fig 1

Fig 1: Abdominal x-ray shows right lower extremity peripherally-inserted central venous catheter (PICC) with tip at around L4/5 level.

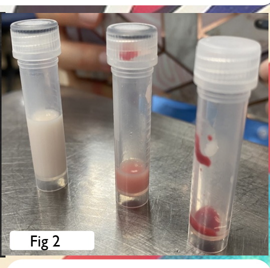
Fig 2

Fig 2: Lumbar puncture yielded abnormal milky content, suspicious for TPN extravasation.

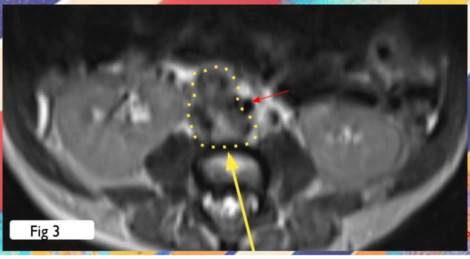
Fig 3

Fig 3: MRI L-S spine T2-weighted axial sequence show loss of normal flow void (dashed area) with irregular distension and mixed T2 heterogeneities of the IVC (yellow arrow). Normal flow void seen in abdominal aorta (red arrow).

Subsequent dedicated MRI venogram and doppler US confirmed extensive infra-renal iliocaval thrombosis with development of secondary venous collaterals (Fig 4-5).

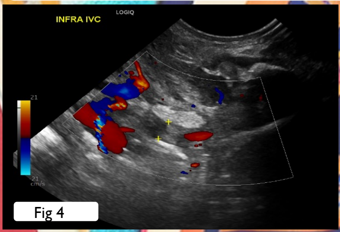

Fig 4

Fig 4 (left): US doppler shows echogenic filling defects in the infra-renal IVC with absence of doppler flow.

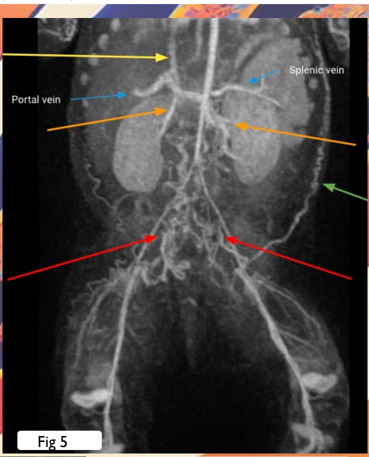

Fig 5

Fig 5 (right): MRI venogram shows absent infra-renal IVC with multiple dilated venous collaterals draining via the deep azygos-hemiazygos pathway (red arrows), as well the superficial pathway (green arrows). Note the normal supra-renal IVC (yellow arrow) and bilateral renal veins (orange arrows)

Why was "milky" aspirate obtained during lumbar puncture?

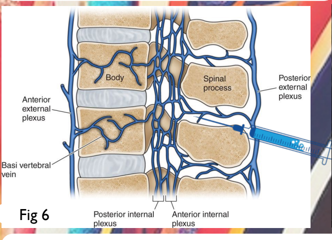

Fig 6

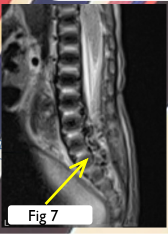
Fig 7

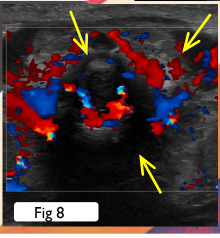
Fig 8

Fig 6: Pictorial diagram of the venous anatomy during a lumbar puncture.
Fig 7: MRI L-S spine sagittal T2-weighted sequence shows dilated epidural venous plexus at lower thecal sac.
Fig 8: US spine shows corresponding dilated epidural and paravertebral venous plexus on doppler imaging.

The plausible explanation for presence of "milky/TPN" aspirate during lumbar puncture was likely related to the puncturing of the abnormally dilated epidural venous plexuses which had led to paucity of accessible CSF space (Fig 6-8) The tip of the PICC inserted through the right lower extremity has also likely entered via the deep paravertebral venous collaterals rather than within the expected IVC location.

Conclusion:
This exhibit presents a rare and peculiar case of iatrogenic neonatal IVC thrombosis, providing an educational radiological review of anatomy, collateral venous pathway systems and the intriguing relationship between atypical clinical presentation and radiological features. A high index of suspicion for underlying deep venous thrombosis should be sought, especially in patients with indwelling vascular catheters, to ensure timely treatment.

Ref: Tieu P, Paes B, Ahmed A, Matino D, Chan A, Bhatt M. Inferior vena cava syndrome in neonates: An evidence-based systematic review of the literature. *Pediatric Blood & Cancer*. 2020;67(4):e28114.